Journal of Biomedical Optics

BiomedicalOptics.SPIEDigitalLibrary.org

Experimental recovery of intrinsic fluorescence and fluorophore concentration in the presence of hemoglobin: spectral effect of scattering and absorption on fluorescence

Vinh Nguyen Du Le
Michael S. Patterson
Thomas J. Farrell
Joseph E. Hayward
Qiyin Fang

SPIE.

Experimental recovery of intrinsic fluorescence and fluorophore concentration in the presence of hemoglobin: spectral effect of scattering and absorption on fluorescence

Vinh Nguyen Du Le,[a] Michael S. Patterson,[a,b] Thomas J. Farrell,[a,b] Joseph E. Hayward,[a,b] and Qiyin Fang[c,*]
[a]McMaster University, Department of Medical Physics and Applied Radiation Sciences, Hamilton, Ontario L8S 4L8, Canada
[b]Juravinski Cancer Centre, Hamilton, Ontario L8V 5C2, Canada
[c]McMaster University, Department of Engineering Physics, Hamilton, Ontario L8S 4L8, Canada

Abstract. The ability to recover the intrinsic fluorescence of biological fluorophores is crucial to accurately identify the fluorophores and quantify their concentrations in the media. Although some studies have successfully retrieved the fluorescence spectral shape of known fluorophores, the techniques usually came with heavy computation costs and did not apply for strongly absorptive media, and the intrinsic fluorescence intensity and fluorophore concentration were not recovered. In this communication, an experimental approach was presented to recover intrinsic fluorescence and concentration of fluorescein in the presence of hemoglobin (Hb). The results indicated that the method was efficient in recovering the intrinsic fluorescence peak and fluorophore concentration with an error of 3% and 10%, respectively. The results also suggested that chromophores with irregular absorption spectra (e.g., Hb) have more profound effects on fluorescence spectral shape than chromophores with monotonic absorption and scattering spectra (e.g., black India ink and polystyrene microspheres). [DOI: 10.1117/1.JBO.20.12.127003]

Keywords: intrinsic fluorescence signal; hemoglobin; optical properties; diffuse reflectance; fluorescence quantum yield.

Paper 150515RR received Aug. 1, 2015; accepted for publication Nov. 12, 2015; published online Dec. 22, 2015.

1 Introduction

Many biological fluorophores in human mucosal tissues, such as collagen, nicotinamide adenine dinucleotide (NADH), and flavin adenine dinucleotide (FAD), can absorb light at shorter wavelengths (e.g., in the ultraviolet region) and emit fluorescence at longer wavelengths (i.e., in the visible region).[1] Their fluorescence properties (e.g., intensity and lifetime) and relative concentration can be used to obtain the status of the studied tissues.[2–9] For example, the fluorescence of NADH and FAD may increase as cells become dysplastic due to the disruption of the extracellular matrix,[2,3] whereas collagen density or concentration increases during tumor progression.[4] However, during *in vivo* measurements, background absorbers and scatterers strongly distort the intrinsic fluorescence and make it difficult to obtain the correct concentration of the fluorophore. The term "intrinsic fluorescence signal" (IFS) was adapted by different research groups to describe the fluorescence without the interference of other absorbers and scatters.[10–12] Details of the physical definition of IFS can be found in Sec. 2.3 of the manuscript. In soft tissues, typical absorbers are hemoglobin (Hb, primary absorber), collagen crosslinks, NADH, and FAD (secondary absorbers), whereas scatterers include cell nuclei, organelles, and collagen fibers.[5] The fluorophore concentration can be extracted only if the effect of absorption and scattering is compensated and the IFS is retrieved.

Many studies have attempted to retrieve the IFS using theoretical modeling, experimental approaches, or a combination of both. For example, Palmer and Ramanujam[13] developed a Monte-Carlo method incorporated with Mie theory and a nonlinear optimization algorithm to recover the IFS of furan dye within 10% error. Kanick et al.[14] extended MC algorithms to investigate the effect of absorption on the measured fluorescence intensity, but the information regarding intrinsic fluorescence and fluorophore concentration was not recovered. MC algorithms were also used to calculate the optical fiber's calibration factor, which was later used to recover the IFS from the measured diffuse reflectance (DR).[12] Although the MC-based method is flexible for different illumination-collection geometries, it requires intensive computation during forward modeling even if modern computational power is applied.[15–21] Therefore, it is necessary to develop a simpler approach that can perform fast recovery of fluorescence and be adapted to different systems. In studies by Diamond et al.,[22] the fluorophore concentration was extracted by applying diffusion theory for the measured fluorescence and DR. However, optical properties extraction based on the diffusion approximation may not be accurate for tumorous tissues with high angiogenesis (such as glioblastoma) or for intraoperative surgery where bleeding is unavoidable. In such case, absorption level usually dominates scattering level, and diffuse approximation becomes inapplicable.[23]

Finlay and Foster[24] used a forward adjoint model of fluorescence to recover the shape of intrinsic fluorescence spectra and Hb absorption with the prior knowledge of concentration of known absorbers and known fluorophores. The approach, however, was not able to retrieve the absolute fluorescence intensity

*Address all correspondence to: Qiyin Fang, E-mail: qiyin.fang@mcmaster.ca

1083-3668/2015/$25.00 © 2015 SPIE

and fluorophore concentration.[24] In studies by Kim et al., an analytical method was developed to correct the fluorescence line shape and fluorophore concentration based on the assumption that fluorescence is in a linear relationship with DR at emission wavelengths.[25] However, such an assumption is valid only if an excitation wavelength within 380 to 450 nm is used so that the migration path of emitted photons is approximately the same as that of reflected photons.[25] Furthermore, previous phantom studies considered furan 2 as the fluorophores[12] and red marking dye as the background absorber.[16] Such materials are not relevant to most tissue investigations, and the fluorescence intensity and fluorophore concentration were not recovered. For example, furan 2 has an emission peak at 400 to 420 nm, whereas many endogenous fluorophores such as NADH, FAD, and elastin have emission peaks at longer wavelengths (450 to 550 nm).[1] Hoy et al. attempted to recover the intrinsic fluorescence line shape of fluorescein based on the recovered optical properties with the single-fiber fluorescence (SFF) technique.[26] However, the fluorescence intensity and fluorophore concentration were not recovered for comparison. Moreover, the validation of SFF was performed on phantoms with high concentrations of intralipid while using 365 nm as the excitation source.[26] A recent report has shown that intralipid fluoresces strongly at this concentration and has a longer fluorescence lifetime (4.5 ns) compared to fluorescein (3.8 to 4 ns).[1,27] Therefore, its fluorescence properties should not be ignored. Although different studies were able to recover the intrinsic fluorescence and concentration of protoporphyrin IX in human skin using excitation light at longer wavelengths from 600 to 800 nm,[28–30] many fluorophores in human mucosa and brain such as NADH, FAD, and collagen absorb light at shorter wavelengths from 350 to 500 nm.[1] Therefore, additional evaluations on phantoms or tissues with Hb as the dominant absorber are necessary if these approaches[28–30] are to be applied to image mucosal tissues or brain tissues.

In this paper, we explored the ability of a simpler approach[31] for fast recovery of fluorescence peaks and fluorophore concentration in highly absorptive media using an excitation wavelength at 355 nm. The approach was validated on tissue-simulating phantoms using fluorescein as fluorophore, polystyrene microspheres as background scatterers, and black India ink and ferrous-stabilized Hb as background absorbers.

2 Methods

2.1 *Tissue-Simulating Phantoms*

Stock solution of fluorescein with a concentration of 10^{-3} M was prepared by dissolving fluorescein powder (46955-100G-F, Sigma-Aldrich, Missouri) in concentrated ethanol 95% (Commercial Alcohols, GreenField Specialty Alcohol Inc., Ontario, Canada). Fluorescein concentrations of 10^{-4} and 10^{-5} M were prepared by simply diluting the stock solution in deionized (DI) water. The absorption and emission spectra of fluorescein are extremely sensitive to alcohol residue, and careful sample preparation is necessary to obtain accurate measurements.[27] To simulate tissue scattering, polystyrene microspheres with diameter of 1 μm (07310-15, Polysciences Inc., Pennsylvania) were used. These spheres were preferred because their scattering properties are similar to biological tissues, and their well-controlled size, index of refraction,[17,18,32] and accurate estimation of scattering properties are calculated using Mie theory.[33–35] To investigate the effect of scattering on fluorescence, six phantoms (S1 to S6) with six different concentrations of microspheres (from 0.05% to 0.72% w/v) were created. These concentrations were obtained by diluting the original concentration of 2.65% w/v in DI water.[27]

To simulate tissue absorption, both black India ink (Higgins Ink, Chartpak Inc., Massachusetts) and Hb (H0267, Sigma-Aldrich, Missouri) were used. Black India ink is widely used to simulate absorbers in tissue optics because of its similar exponential decrease of absorption with wavelength as that of NADH and FAD, its low cost, spectral stability, and low fluorescence activity.[2,5,36–40] Applying the same assumption made by previous studies,[38,40] the current study treated India ink as a pure absorber. Absorption and scattering coefficients of black India ink and microspheres are shown in Sec. 3.2. Ferrous-stabilized Hb was selected because its absorption spectrum is close to that of human blood,[18] and due to its high and stable oxygen saturation (~100%).[33,41] Absorption coefficients of Hb phantoms are shown in Sec. 3.1. A stock solution with Hb concentration of 30 mg/ml was prepared by diluting Hb powder in DI water.

To observe the effect of Hb absorption on fluorescence, three phantoms with Hb concentrations of 3.5, 10, and 20 mg/ml (Hb3.5, Hb10, and Hb20) and microsphere concentration of 0.4% w/v were produced. To investigate the effects of secondary absorbers on fluorescence, five phantoms (I1 to I5) with various India ink concentrations (0.05% to 0.6%) and microsphere concentration of 0.72% w/v were created. In all phantoms, optical properties were controlled and calculated by applying Beer–Lambert's law to the absorbance of pure solute absorbers (fluorescein, India ink, or Hb) measured with a spectrophotometer (Ultraspec 3000, Pharmacia Biotech Inc., New Jersey) for absorption coefficient (μ_a) and Mie theory for reduced scattering coefficient (μ_s'). Scattering anisotropy (g) of polystyrene microspheres can be found in a previous study.[27] The volume and depth of each phantom were 6 ml and 5.5 cm, respectively. Each phantom was contained in a test tube with diameter of about 12 mm.

2.2 *Instrumentation*

DR signal from the phantoms was generated using a broadband light source (Dolan-Jenner MI-150, Edmund Optics, New Jersey) for illumination, whereas steady state fluorescence (SSF) signal was generated using a solid-state laser (PNV-001525-140, Teem Photonics, Meylan, France) at 355 nm with 300-ps full width at half maximum for excitation. Measurements of both DR and SSF signals were performed with the same customized optical probe.[42] Figure 1 shows the geometry of the optical probe, including a DR/SSF source fiber; different DR/SSF detection fibers bundled into three groups at three source–detector distances (SDD) of 0.23, 0.59, and 1.67 mm; and a center fiber for time-resolved fluorescence (TRF) measurement. Three spectrometers (UV-NIR-200, StellarNet Incorporation, Tampa, Florida) were used to record the reflectance signal and SSF signal and were controlled by a moderately equipped computer (IBM Core 2 Duo L7500, 2 GB RAM). The position of the fiber probe was unchanged during both measurements. This enabled the correction of fluorescence using the DR measured at the same location.

Later, the fluorescence lifetime of fluorescein in each phantom was recorded using center optical fiber with a core diameter of 400 μm and numerical aperture of 0.12 (Fig. 1) and a calibrated acousto-optic tunable filter-based time-resolved

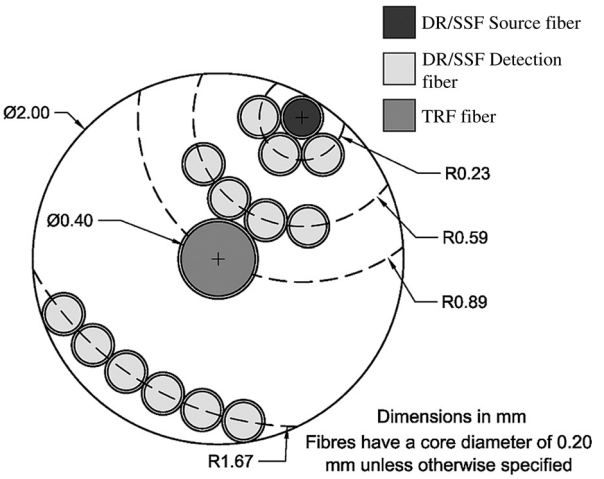

Fig. 1 Schematics of the fiber probe geometry. Diffuse reflectance/steady-state fluorescence (DR/SSF) detection fibers are bundled together into three groups, each at the indicated distance (0.23, 0.89, and 1.67 mm) from the DRS/SSF source fiber (measured from the center of each fiber). In addition, a central fiber was used for time-resolved fluorescence (TRF) spectroscopy measurements. Diameter of DR/SSF fibers is 200 μm and diameter of the TRF fiber is 400 μm.

spectrometer.[43] Details of the time-resolved system can be found elsewhere.[43,44] In all measurements, the fiber-optic probe was held perpendicular to the phantom surface and slightly touched the phantoms. The time-resolved measurements merely served as a secondary verification of the stability and consistency in fluorescence properties of fluorescein in all phantoms (the primary verification was spectrometer measurement of absorbance spectra) and had no role in retrieving fluorescein concentration. In the current study, experimental measurements with India ink and microspheres were performed on different days with different batches and concentrations of fluorescein. Therefore, consistency in our time-resolved measurements would also ensure that the use of additional absorbers and scatterers did not alter the chemical structure of fluorescein and that the same alcohol concentration was present in all the phantoms.

2.3 *Retrieving of Intrinsic Fluorescence*

When the excitation light with intensity I_x was used to illuminate the sample, fluorescence was emitted with a spectral distribution $f_{xm}(\lambda_m)$. However, due to absorption and scattering in the tissue sample, only a fraction of f_{xm}, defined as $F_{xm}(\lambda_m)$, was collected. The subscripts x and m indicate the dependence of the quantity on excitation and fluorescence emission wavelengths (λ_x and λ_m), respectively. Hence, F_{xm} and f_{xm} represent the measured fluorescence and intrinsic fluorescence at emission wavelength m due to excitation wavelength x, respectively. Müller et al. and Zhang et al. defined f_{xm} as the total fluorescence intensity of a thin slab of thickness l (cm) of a material that does not absorb or scatter photons while containing the same concentration of fluorophores.[12,16,31] In a closed form, f_{xm} can be written in terms of Eq. (1), where μ_{afx} is the absorption coefficient (cm^{-1}) due only to the slab's fluorophore at excitation wavelength x, and ϕ_{xm} (dimensionless) is the fluorescence quantum yield.[12,16,31]

$$f_{xm} = \frac{\lambda_x}{\lambda_m} I_x l \mu_{afx} \phi_{xm}. \tag{1}$$

In Eq. (1), ratio λ_x/λ_m corrects for the difference in photon energy at excitation and emission wavelength, whereas the product $l\mu_{afx}$ ($\ll 1$) represents the probability of a photon at excitation wavelength λ_x to be absorbed by the fluorophore, and ϕ_{xm} represents the probability of a photon at emission wavelength λ_m to be generated after the absorption event at λ_x. μ_{afx} can be defined as $c\varepsilon\ \ln(10)$, where c is fluorophore molar concentration (M) and ε extinction coefficient ($\mathrm{cm}^{-1}\,\mathrm{M}^{-1}$) at λ_x. Because f_{xm} directly relates to c, Eq. (1) can be rewritten in the form of Eq. (2) with a consideration of a mixture of i fluorophores:

$$f_{xm} = \frac{\lambda_x}{\lambda_m} I_x l\ \ln(10) \sum_i \varepsilon_i c_i \phi^i_{xm}. \tag{2}$$

By using the escape probability distribution function (ρ), the phase-function dependence of the scattering was separated from the scattering and absorption coefficients, and the diffuse reflectance (R) and the measured fluorescence (F_{xm}) can be modeled using Eqs. (3) and (4).[12,31]

$$R = \sum_{n=1}^{\infty} \rho_n w_n, \tag{3}$$

$$F_{xm} = \sum_{n=1}^{\infty} \sum_{i=0}^{n-1} \rho_{ni} w_{ni}, \tag{4}$$

where $w_n = a^n = [\mu_s/(\mu_a + \mu_s)]^n$, $w_{ni} = a_x^{i+1}(f_{xm}/\mu_{sx})a_m^{n-i-1}$, and $\rho_n = R_0[e^{S(1-g)} - 1]e^{-nS(1-g)}$.

In Eqs. (3) and (4), n is the number of scattering events (dimensionless), S is a constant calibration factor for each individual fiber (dimensionless), w is the photon weight (dimensionless), a is the albedo (dimensionless), μ_a is the absorption coefficient (cm^{-1}), μ_s is the scattering coefficient (cm^{-1}), g is the anisotropy parameter (dimensionless), and R_0 is the diffuse reflectance from a standard sample containing only scatterers (dimensionless). By combining the expressions of R and F_{xm} into Eq. (1), a relationship between f_{xm} and F_{xm} can be written as Eq. (5).

$$f_{xm} = \frac{\mu_{sx} * l * F_{xm}}{\left\{\frac{R_{0x}R_{0\,m}}{[e^{S(1-g_x)}-1][e^{S(1-g_m)}-1]}\right\}^{1/2} \frac{R_{tx}}{R_{0x}} \left\{\frac{R_{tm}}{R_{0\,m}} + [e^{S(1-g_m)} - 1]\right\}}. \tag{5}$$

In Eq. (5), R_t is the diffuse reflectance from the targeted samples. In the studied phantoms, μ_s and g were obtained by applying Mie theory for specific microsphere diameter and concentration.[27] To calculate the diffuse reflectance R, the measured reflectance intensity of the sample $I_{\mathrm{r,sample}}$ was normalized to the reflectance intensity of a standard spectralon sample with 99.9% reflectivity $I_{\mathrm{r,std}}$ (Labsphere, Inc., New Hampshire) after subtracting the background signal intensity $I_{\mathrm{r,bg}}$. This method is described via Eq. (6).

$$R = \frac{I_{\mathrm{r,sample}} - I_{\mathrm{r,bg}}}{I_{\mathrm{r,std}} - I_{\mathrm{r,bg}}}. \tag{6}$$

The retrieved signal f_{xm} in Eq. (5) can be used to recover the concentration of fluorophore for a known value of ϕ_{xm}. In the current study, fluorescence quantum yield of fluorescein in basic

ethanol was assumed to be 0.97 at emission peak.[45,46] In experimental measurement, due to the strong intensity of the laser, a neutral density filter with optical density of 2 and a short exposure time (~1 ms) was applied when measuring I_x to avoid saturation at spectrometers. Therefore, to enable accurate estimation of c from Eq. (2), a correction factor k was applied so that $k = 10^{-2}(1/1130)$, where $1/1130$ is the ratio of exposure time used for I_x and for F_{xm} (or f_{xm}). The concentration c of fluorescein in the phantom can be experimentally estimated in Eq. (7):

$$c = k\frac{f_{xm}\lambda_m}{I_x\lambda_x l\varepsilon\phi_{xm}\ \ln(10)}. \tag{7}$$

To obtain the calibration factors l and S in Eq. (5), the least squares fitting routine fminsearch() in MATLAB® was used to fit the measurement of f_{xm} (from the reference nonscattering phantom), F_{xm}, and R_{xm} of calibration phantoms into Eq. (5). This optimization method is based on the Nelder–Mead simplex algorithm and has been widely used for spectral analysis in spectral imaging.[47–49] In the fitting routine, the ideal intrinsic fluorescence f_{xm} was measured directly on a phantom consisting solely of fluorescein 10^{-4} M (in DI water), whereas F_{xm} and R_{xm} were measured with phantoms consisting of fluorescein 10^{-4} M and various India ink and microsphere concentrations. To simplify the fitting routine, l was set at 1 cm. Fitting routines for known spectra of f_{xm}, F_{xm}, and R_{xm} yielded values of 54.6, 45.5, and 48.2 for fibers with an SDD of 0.23, 0.59, and 1.67 mm, respectively. These S values were later used to retrieve f_{xm} in Hb phantoms.

Similar to previous methods,[12,31] the current method utilized the ideas that enabled the retrieving of intrinsic fluorescence from the measured DR. The main difference lies in the calibration approaches. The current method incorporated system characteristics such as light source intensity and position of the fiber probe into the calibration. Therefore, the current method enabled recovery of absolute fluorescence intensity via Eq. (5) and of fluorophore concentration via Eq. (7), whereas the previous methods could recover only the relative fluorescence intensity and spectral shape.

3 Results

3.1 *Effect of Hemoglobin Absorption on Fluorescence*

Figure 2 shows μ_a of Hb and fluorescein, as well as μ_s' of polystyrene microspheres used in the Hb-based phantoms (Hb3.5, Hb10, and Hb20). In these phantoms, the concentration of fluorescein and microspheres remained the same, whereas Hb concentration was varied. The inset of Fig. 2(b) shows that the measured μ_a was in excellent agreement with reference μ_a values for fluorescein 10^{-4} M in alcohol.[45,50] The reference μ_a was calculated by multiplying fluorescein concentration to that of its tabulated molar extinction coefficients.[50] As indicated elsewhere, an Hb concentration of 3.5 mg/ml best simulates background absorption in mucosal tissue.[18] In addition, a microsphere concentration of 0.4% w/v (~0.0073 spheres per cubic micrometer) was used to simulate background scattering.

Figure 3(a) shows the measured SSF (F_{xm}) from three phantoms using SDD of 0.59 mm. Due to the similarity in the measured fluoresence spectra at different fibers, only the signal at one fiber is shown [Fig. 3(a)]. In general, increasing absorption (from 3.5 to 20 mg/ml) decreases the measured fluorescence intensity due to the decrease in the number of emitted photons escaping to the tissue surface. To compare the spectral shapes, the fluorescence spectrum of fluorescein in DI water (instrinsic) and in Hb and microspheres (distorted) is shown in the same graph [Fig. 3(b)]. As shown in Fig. 3(b), the spectral shape of the measured fluorescence was highly distorted in the wavelength regions where Hb strongly absorbs photons (540 nm and 580 nm). Figure 3(c) shows examples of the absorption dependence of the measured fluorescence at the fluorescein emission peak of 520 nm.

Despite the distortion in the measured SSF, it was observed that average lifetime in the phantoms remains unchanged, indicating that lifetime was not affected by background absorption (Fig. 4). A biexponential deconvolution method was used to obtain the lifetime information of the measured fluorescence signals.[43] Figure 4(a) shows that fluorescence lifetime is consistent at the emission wavelength for a phantom with Hb concentration of 3.5 mg/ml. In addition, Fig. 4(b) shows that the fluorescence lifetime of fluorescein in Hb phantoms agreed with that of the intrinsic signal within one standard deviation. In Fig. 4(b), the fluorescence lifetime was averaged over six repeated measurements, and standard deviations were calculated and shown as error bars.

Figure 5(a) shows the corresponding DR of three Hb-based phantoms using SDD of 0.59 mm. In general, the drops of reflectance at the 540 and 580 nm regions were due to Hb absorption in these regions [Fig. 2(a)], whereas the drop at 470 to 520 nm was mainly due to fluorescein absorption [Fig. 2(b)]. Figures 5(b) and 5(c) compare the measured fluorescence (F_{xm}) to that of recovered and intrinsic fluoresence for a phantom with Hb concentration of 3.5 mg/ml using SDD of 0.59 mm. The recovered fluoresence (f_{xm1}) is the fluorescence signal calculated using Eq. (5). The least-square fitting routine fminsearch() was also applied to fit f_{xm1} to the shape of the intrinsic spectrum (ideal) and obtain the fitted spectrum f_{xm2} of f_{xm1}. The square errors between f_{xm1} and f_{xm2} were used to optimize the results of the fitting. Figure 5(d) compares the percentage difference among F_{xm}, f_{xm1}, and f_{xm2} with respect to the ideal intrinsic fluorescence for phantom Hb3.5 (Hb concentration of 3.5 mg/ml).

On average over 480 to 620 nm, the percentage error was ~81%, 24%, and 8% for F_{xm}, f_{xm1}, and f_{xm2}, respectively.

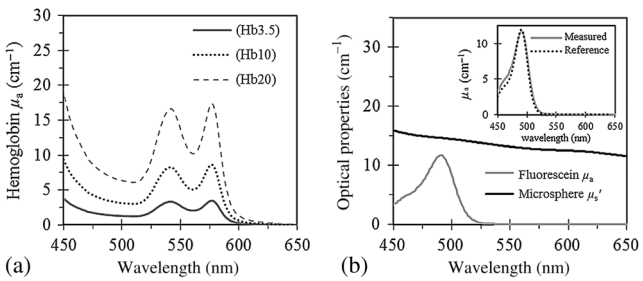

Fig. 2 (a) Absorption coefficients μ_a of hemoglobin (Hb) phantoms (Hb3.5: 3.5 mg/ml, Hb10: 10 mg/ml, and Hb20: 20 mg/ml) as a function of wavelength and (b) reduced scattering coefficients μ_s' of polystyrene microspheres and μ_a of fluorescein as a function of wavelength. In these phantoms, the concentration of microsphere and fluorescein was kept constant at 0.4% w/v and 10^{-4} M, respectively. The inset in (b) compares μ_a of fluorescein 10^{-4} M measured in the current study (measured) to that extracted from the literature (reference).[50]

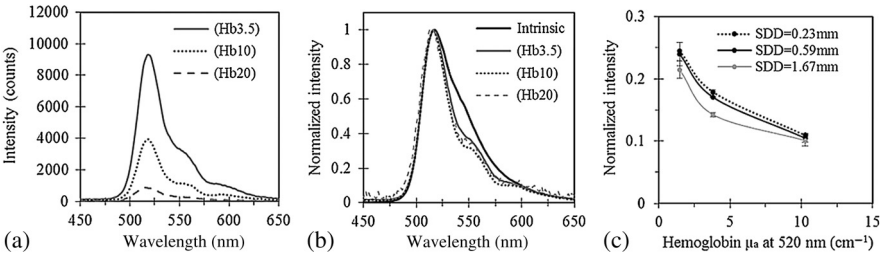

Fig. 3 (a) Measured fluorescence (F_{xm}) of phantoms (Hb3.5, Hb10, and Hb20), (b) normalized emission spectra, and (c) normalized intensity as a function of μ_a at the emission peak 520 nm for all three collection distances. In (c), the intensity at the emission peak of phantoms was normalized to that of the sample consisting solely of fluorescein 10^{-4} M in deionized water (DI) water (intrinsic). In all cases, the concentration of fluorescein was 10^{-4} M; microsphere was 0.4% w/v, respectively; and SDD of 0.59 mm was used.

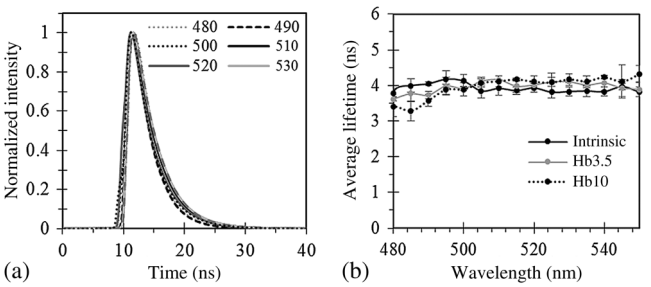

Fig. 4 (a) Fluorescence lifetime for phantom (Hb3.5) at selected emission wavelengths and (b) average fluorescence lifetime of the phantoms (Hb3.5 and Hb10). The intrinsic signal was collected using fluorescein 10^{-4} M in diluted ethanol without additional scatterer or absorber.

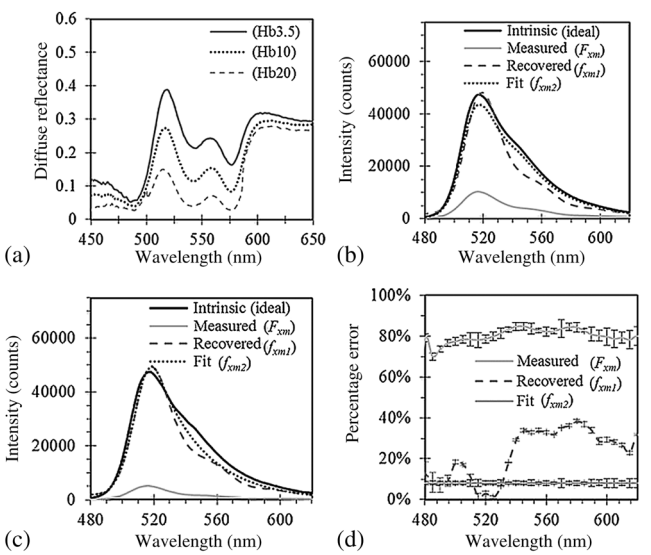

Fig. 5 (a) DR of the phantoms Hb3.5, Hb10, and Hb20; (b) measured fluorescence (F_{xm}), the retrieved fluorescence (f_{xm1}), the fitted fluorescence (f_{xm2}), and the ideal intrinsic fluorescence for phantoms with Hb concentrations of 3.5 mg/ml and (c) of 10 mg/ml; (d) Absolute percentage difference in signal intensity with respect to the ideal intrinsic signal for Hb3.5 phantom. In all cases, fluorescein concentration of 10^{-4} M, microsphere concentration of 0.4% w/v, and SDD of 0.59 mm were used. In (b) and (c), F_{xm} is fluorescence under the influence of Hb absorption and microsphere scattering, whereas f_{xm1} is the recovered fluorescence using Eq. (3), f_{xm2} is the fitted spectrum of f_{xm1}, and the intrinsic signal is the signal measured in ideal conditions in which the phantom consists solely of fluorescein 10^{-4} M in DI water.

These numbers were 91%, 26%, 9% and 99%, 30%, 13% for phantoms Hb10 and Hb20, respectively (Table 1). On average over 480 to 620 nm, the accuracy of the signal was improved by 70% without fitting and by 90% with fitting. Considering only peak emission at 522 nm, the percentage errors of F_{xm}, f_{xm1}, and f_{xm2} are 79%, 3%, and 8%, respectively. The recovered fluorescence at 522 nm was used to calculate the concentration of fluorescein using Eq. (7). With x of 355 nm (excitation peak) and m of 522 nm (emission peak), the values of I_{355} and $f_{355,522}$ are 61225 counts and 45093 counts, respectively. The extinction coefficient ε_{355} of fluorescein was assumed to be 0.04 $cm^{-1}\,M^{-1}$,[50] and $\phi_{355,522}$ was assumed to be 0.97.[45] Therefore, the c value of $1.07 * 10^{-4}$ M was estimated using Eq. (7). Table 2 summarizes the extracted concentration of fluorescein in three Hb phantoms. On average, the extracted concentration was within 10% of the controlled value of 10^{-4} M.

3.2 *Effect of India Ink Absorption on Fluorescence*

To further investigate the absorption effect on fluorescence, black India ink with increasing concentration from phantoms I1 to I5 was used to simulate background absorption and a microsphere concentration of 0.72% was used to simulated background scattering. Figure 6 summarizes the optical properties of the phantoms used in this section. The goal of this subsection is to investigate the effects of a monotonic decreasing absorption on fluorescence intensity and spectral shape, and to compare it to the Hb cases.

Figure 7(a) summarizes the measured fluorescence (F_{xm}) from phantoms I1 to I5, whereas Fig. 7(b) compares the spectral shape of F_{xm} and f_{xm}, and Fig. 7(c) summarizes the corresponding R. These data were collected at SDD = 0.59 mm. A similar trend to that of Fig. 3(a) was observed in Fig. 7(a):

Table 1 Average percentage difference (AVG) of F_{xm}, f_{xm1}, f_{xm2} with respect to the ideal intrinsic fluorescence over 490 to 620 nm. Analysis for all three phantoms (Hb3.5, Hb10, and Hb20) is shown.

Quantity	Percentage error (%) for each phantom		
	Hb3.5	Hb10	Hb20
F_{xm}	80.8 ± 2.7	91.3 ± 1.8	98.7 ± 0.4
f_{xm1}	24.1 ± 12.4	26.3 ± 11.4	29.6 ± 11.1
f_{xm2}	8.1 ± 1.5	8.5 ± 0.8	12.8 ± 1.1

Table 2 The recovered fluorescein concentration (c) in three hemoglobin (Hb) phantoms from Eq. (5). The controlled concentration of fluorescein in these phantoms was 10^{-4} M.

Quantity	Phantom		
	Hb3.5	Hb10	Hb20
$f_{355,522}$ (counts)	45,093 ± 786	49,958 ± 232	44,174 ± 317
$F_{355,522}$ (counts)	9472 ± 165	4527 ± 21	557 ± 4
***c* (M)**	**1.07E−04**	**1.19E−04**	**1.05E−04**
	4.E − 06	2.E − 06	2.E − 06

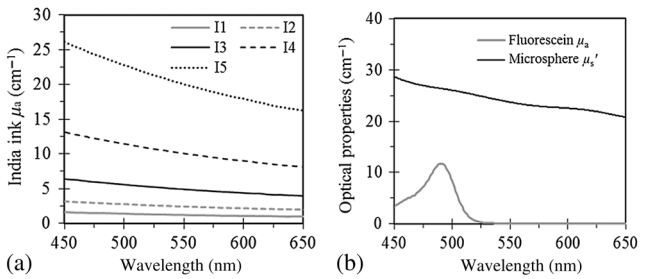

Fig. 6 (a) Absorption coefficients μ_a of the India ink in phantoms I1 to I5 as a function of wavelength and (b) reduced scattering coefficients μ_s' of polystyrene microsphere and μ_a of fluorescein as a function of wavelength. In these phantoms, the concentration of India ink increased from phantom I1 to I5, and the concentration of microsphere and the fluorescein was kept constant at 0.72% w/v and 10^{-4} M, respectively.

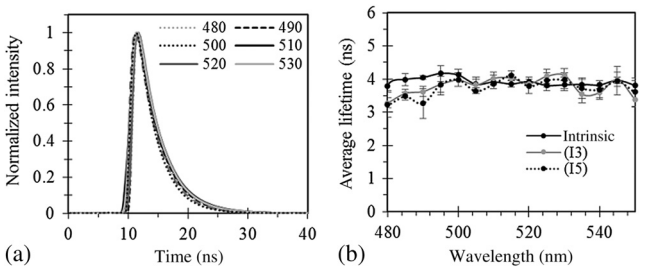

Fig. 8 (a) Fluorescence lifetime for phantom (I3) at selected emission wavelengths and (b) average lifetime of the phantoms (I3 and I5) at emission wavelength. The intrinsic signal was collected using fluorescein 10^{-4} M in diluted ethanol without additional scatterer or absorber.

SSF decreases as absorption increases. However, there is a significant difference between Figs. 3(b) and 7(b): the spectral shape of the fluorescence for phantoms with ink as background absorber was not distorted and remained similar to that of the intrinsic signal (measured with only fluorescein in DI water). This can be explained by referring to either the India ink absorption spectra [Fig. 6(a)] or the phantom DR spectra [Fig. 7(c)]. Similar to the Hb phantom cases, increasing absorption (from I1 to I5) decreases the reflectance signal collected [Fig. 7(c)]. However, in contrast to the Hb phantoms, there are no peaks in the India ink absorption spectra [Fig. 6(a)] or DR spectra [Fig. 7(c)]. Note that the drop of DR at 500 nm in Fig. 7(c) was due to the strong absorption of fluoresecein at this region. Again, Eq. (7) can be applied to extract fluorescein concentration. An average error of 5% was obtained for the recovered fluorescein concentration (Table 3). Furthermore, the fluorescence lifetime of India ink phantoms remained the same as that of the intrinsic signal, as expected (Fig. 8). Table 4 provides a brief summary of the average fluoresence lifetime of fluorescein in Hb and India ink phantoms over the emission region of

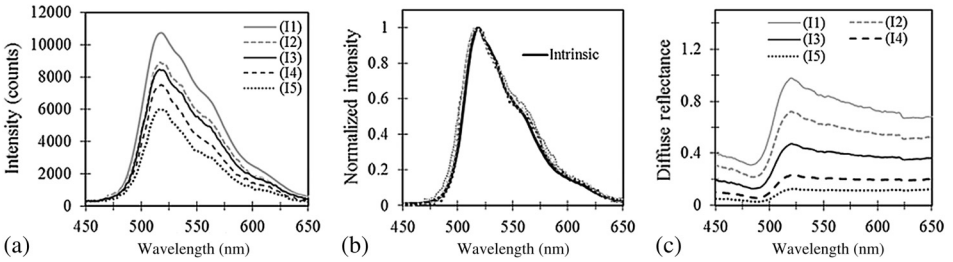

Fig. 7 (a) Measured fluorescence emission spectra of the phantoms (I1 to I5), (b) normalized fluorescence emission spectra, and (c) the corresponding DR spectra. These data were collected with the fiber at SDD = 0.59 mm. In all phantoms, fluorescein concentration was 10^{-4} M.

Table 3 The recovered fluorescein concentration in ink-microsphere phantoms. The controlled concentration of fluorescein in these phantoms was 10^{-4} M.

Quantity	Phantom				
	I1	I2	I3	I4	I5
$f_{355,522}$ (counts)	43,652 ± 741	46,230 ± 420	46,589 ± 744	42,442 ± 837	41,342 ± 823
$F_{355,522}$ (counts)	10,479 ± 149	8778 ± 58	8282 ± 112	7281 ± 115	5918 ± 93
***c* (M)**	**1.04E−04**	**1.10E−04**	**1.11E−04**	**1.01E−04**	**9.84E−05**
	3.E − 06	2.E − 06	3.E − 06	3.E − 06	3.E − 06

Table 4 Overall average lifetime of fluorescein in different phantoms (in region 480 to 550 nm). Concentration of fluorescein in these phantoms was 10^{-4} M. Concentration of microspheres was 0.4% w/v and 0.72% w/v in Hb and India ink phantoms, respectively.

Quantity	Phantom						
	Intrinsic	Hb3.5	Hb10	Hb20	(I3)	(I4)	(I5)
τ (ns)	3.92 ± 0.12	3.96 ± 0.16	3.97 ± 0.31	3.95 ± 0.32	3.78 ± 0.26	3.84 ± 0.25	3.74 ± 0.26

480 to 550 nm. Overall, the fluoresence lifetime remained constant and agreed with previously reported values for fluorescein in diluted alcohol.[1]

3.3 *Effect of Microsphere Scattering on Fluorescence*

Figure 9 summarizes the optical properties of phantoms S1 to S6. In these phantoms, microsphere concentration increases from S1 (0.05% w/v) to S6 (0.72% w/v) [Fig. 9(a)], whereas the concentration of fluorescein is kept constant at 10^{-5} M. No other absorbers were added. Figure 9(b) shows the μ_a spectrum of fluorescein 10^{-5} M solution. The goal of this subsection is to inspect the effects of a monotonically decreasing reduced scattering on fluorescence intensity and spectral shape.

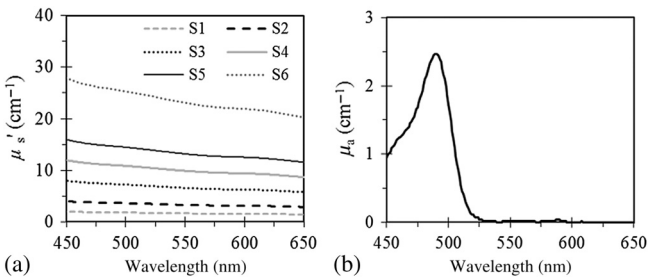

Fig. 9 (a) Reduced scattering coefficients μ_s' and (b) absorption coefficients μ_a of phantoms S1 to S6. In these phantoms, the concentration of microspheres increased from phantoms S1 to S6, whereas the concentration of fluorescein was kept at 10^{-5} M. No other absorbers were added.

The measured SSF of the phantoms is shown in Fig. 10 for all collection distances: 0.23 mm [Fig. 10(a)], 0.59 mm [Fig. 10(b)], and 1.69 mm [Fig. 10(c)]. In general, adding microspheres decreased the fluorescence intensity at first due to the effect of scattering (intrinsic versus S1). The fluorescence intensity eventually increased if more microspheres were added from S1 to S6. Figure 11(a) further illustrates this trend by plotting the normalized intensity at the emission peak as a function of μ_s' (at 520 nm). This phenomenon was consistent with what was reported previously.[12] To compare the intensity trend between SDDs, the fluorescence collected at each SDD was normalized to the intrinsic fluorescence at the same SDD [Fig. 11(a)]. The current results indicated that increasing SDD from 0.23 to 0.59 mm might increase the fluorescence signal up to 40% in highly scattering media, although further increasing of SDD showed the reverse [Fig. 11(a)].

The corresponding DR of phantoms for SDD = 0.59 mm is also shown in Fig. 11(b), and the normalized measured

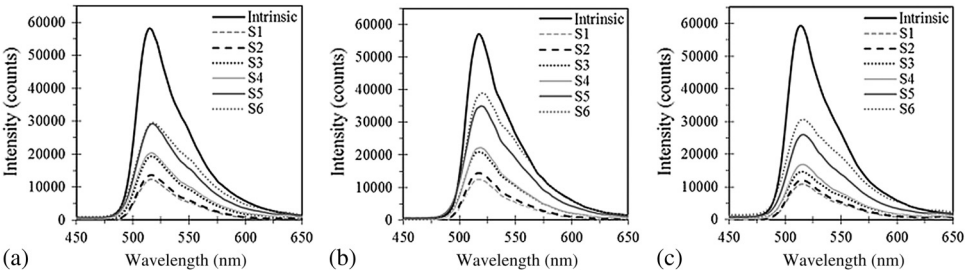

Fig. 10 Measured fluorescence emission spectra of the phantoms using (a) SDD = 0.23 mm, (b) SDD = 0.59 mm, and (c) SDD = 1.67 mm. Microsphere concentration increased from sample S1 to sample S6. Fluorescein concentration was kept constant at 10^{-5} M.

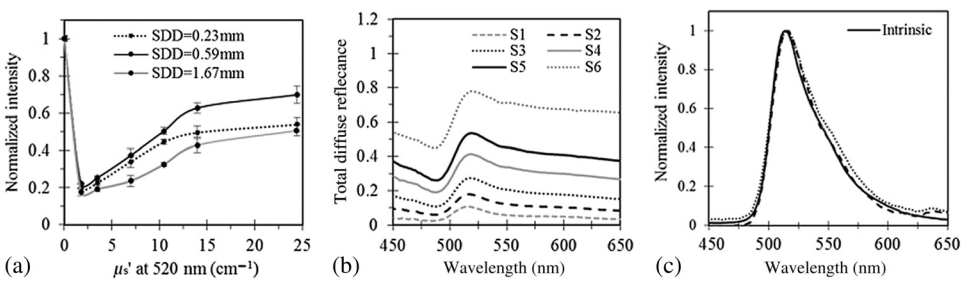

Fig. 11 (a) Normalized fluorescence intensity as a function of μ_s' at emission peak of 520 nm for all three SDDs, (b) corresponding total DR spectra at SDD = 0.59 mm, and (c) normalized fluorescence intensity. Fluorescein concentration was kept constant at 10^{-5} M.

Table 5 The extracted fluorescein concentration (c) in microsphere phantoms from Eq. (5). The controlled concentration of fluorescein in these phantoms was 10^{-5} M.

Quantity	Phantom					
	S1	S2	S3	S4	S5	S6
$f_{355,522}$ (counts)	40,550 ± 1247	51,902 ± 872	43,682 ± 945	54,050 ± 462	49,208 ± 1145	51,367 ± 916
$F_{355,522}$ (counts)	10,036 ± 211	10,998 ± 178	13,493 ± 258	15,688 ± 160	24,617 ± 377	29,294 ± 236
***c* (M)**	**9.05E−06**	**1.16E−05**	**9.75E−06**	**1.21E−05**	**1.10E−05**	**1.15E−05**
	6.E − 07	4.E − 07	4.E − 07	2.E − 07	4.E − 07	3.E − 07

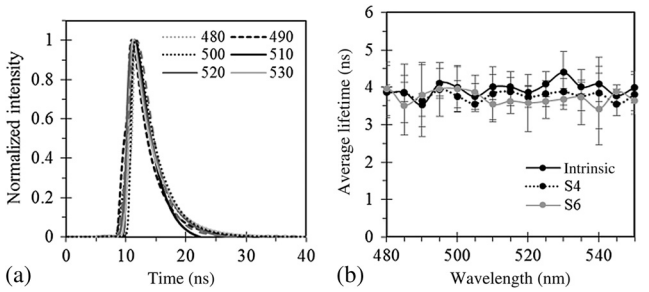

Fig. 12 (a) Fluorescence lifetime for phantom S6 at selected emission wavelengths and (b) average lifetime of the phantoms S4 and S6 at emission wavelength. The intrinsic signal was collected using fluorescein 10^{-5} M in diluted ethanol without additional scatterer or absorber.

fluorescence and intrinsic signal is plotted in Fig. 11(c). In general, increasing scattering increases the probability of detection, thus increasing the reflectance intensity to be collected by the detection fiber [Fig. 11(b)]. This is a reversed trend of increasing absorption in India ink cases [Fig. 7(c)]. Similar to the India ink cases, the spectral shape of the fluorescence in microsphere phantoms remains unchanged [Fig. 11(c)]. The India ink absorption coefficient and microsphere-reduced scattering coefficient are related to wavelength in the form of $\mu = a\lambda^{-b}$, where a and b are positive fitting coefficients, λ is the wavelength, and μ represents absorption coefficients in the India ink case and reduced scattering coefficients in the microsphere case.[34,35] Therefore, the results shown in Figs. 7(b) and 11(c) might indicate that exponential decrease of scattering or absorption with increasing wavelengths does not have effects on the fluorescence spectral shape. Equation (7) was applied to retrieve the concentration of fluorescein in the phantoms S1 to S6, considering SDD = 0.59 mm, exposure time ratio of 1/11700, and I_x value of 63056 counts. As shown in Table 5, an average percentage error of 8% was observed in the recovered fluorescein concentration. In addition, the fluorescence lifetime remained within the standard deviation (Fig. 12). Table 6 provides an overall summary of the average lifetime in regions from 480 to 550 nm for phantoms S1 to S6.

4 Discussion and Conclusions

The current study has shown that Hb absorption strongly distorted the fluorescence spectra of fluorescein at emission wavelength regions near 540 and 580 nm. Most endogenous fluorophores in human tissues emit in this wavelength region upon irradiation with ultraviolet light.[1] Using the proposed method and the constructed phantoms with optical property ranges reported for mucosal tissues and brain tissues (μ_a of 1.2 to 20 cm^{-1} and μ_s' of 1.7 to 24.5 cm^{-1} at 540 nm),[2,5,18,33–35,51,52] fluorescein concentration was recovered with an average error of 10% (Fig. 5, Table 1), considering only the emission peak at 522 nm. On average over 450 to 650 nm, the intrinsic fluorescence intensity of fluorescein was recovered with an error of 27% (versus 90% with raw signal). Although spectral fitting reduced error in recovering fluorescence by 66% on average over 450 to 650 nm, the percentage error of fitted data was higher than that of nonfitted data at the emission peak 522 nm (3% versus 8%). Although absorption affects fluorescence and DR differently due to the difference in light path shown in Eqs. (3) and (4), this difference was accounted for in Eq. (5). In addition, the absorption distortion on the f_{xm2} line shape was accounted for by the ratio of R_{tm}/R_{0m} in Eq. (1).[12] The proposed method was also efficient in retrieving fluorescein's concentration in India ink and microsphere phantoms with an average percentage error of 5% and 8%, respectively (Tables 3 and 4). The current approach used the same concept as previous studies to the extent to which the measured DR was used to compensate the effect of Hb absorption on fluorescence signal.[12,31] What made our approach unique were the abilities to recover absolute fluorescence intensity and to estimate fluorophore concentration via the experimental calibration of individual fibers without the expense of complicated computation. Our ultimate goal is to recover fluorophore concentration using DR and fluorescence measurements and optical properties of the targeted volume. In this manuscript, we demonstrated that the proposed method is feasible to recover fluorophore concentration if

Table 6 Overall average lifetime in region 480 to 550 nm of fluorescein for phantoms S1 to S6.

Quantity	Phantom						
	Intrinsic	S1	S2	S3	S4	S5	S6
τ (ns)	3.96 ± 0.20	3.85 ± 0.18	3.69 ± 0.20	3.73 ± 0.19	3.81 ± 0.12	3.71 ± 0.21	3.72 ± 0.18

optical properties are known. In the next step, an inverse solution is being developed to recover optical properties and to demonstrate that this approach is able to perform real-time tissue measurement. This addition will make the current approach more practical in studying tissue samples. Although a single fluorophore was used in our study, this should not limit the application of the proposed method in media with multiple fluorophores. As demonstrated in the current study, the recovered intensity at the emission peak is crucial to extract fluorophore concentration. In biological tissues, each fluorophore (NADH, FAD, and collagen) has a known emission peak, which can be recovered using Eq. (1), allowing extraction of its concentration via Eq. (7). Although Müller and Hendriks[16] were unable to recover fluorophore concentration, their studies demonstrated the ability of the proposed method to recover multiple fluorescence peaks via Eq. (1).

The current results also show that scattering and absorption materials whose attenuation coefficients decay exponentially with wavelengths (such as black India ink and polystyrene microspheres) have a minor effect on the spectral shape of the fluorescence [Figs. 7(b) and 11(c)]. These observations were made when studying the broadband emission signal of fluorescein in 500 to 625 nm. This finding might indicate that absorption and scattering from NADH, FAD, and collagen fibers do not have significant effects on the fluorescence spectral shape because their attenuation coefficients decay exponentially with wavelength, similar to those of India ink or microspheres.[2,5,34] Therefore, Hb is the only absorber of concern. In addition, a consistency in the average fluorescence lifetime measured with the time-resolved system verified that the chemical structure of fluorescein was not affected by the introduction of India ink, microspheres, or Hb. Furthermore, the current results suggested that increasing SSD from 0.23 to 0.59 mm has the potential to increase the fluorescence signal in highly scattering media, especially for S4 to S6 [Fig. 11(a)]. Therefore, a small increase in collection distance could increase the probability of detection. However, a larger increase of SDD would decrease the probability of an emitted photon reaching the detection fiber. As a result, fluorescence intensity was high at SDD of 0.59 mm and low at SDD of 1.67 mm. Additional theoretical analysis is necessary to confirm this result and to optimize the design to maximize the measured fluorescence signal.

Acknowledgments

The authors would like to thank professor Leyla Soleymani of the Department of Engineering Physics at McMaster University for access to her laboratory during phantom fabrication. This project was supported in part by the Natural Sciences and Engineering Research Council (NSERC) of Canada and Canadian Cancer Society Research Institute (CCSRI). Q. F. holds the Canada Research Chair in Biophotonics at McMaster University.

References

1. M. Y. Berezin and S. Achilefu, "Fluorescence lifetime measurements and biological imaging," *Chem. Rev.* **110**(5), 2641–2684 (2010).
2. R. Drezek et al., "Autofluorescence microscopy of fresh cervical-tissue sections reveals alterations in tissue biochemistry with dysplasia," *Photochem. Photobiol.* **73**(5), 636–641 (2001).
3. I. Pavlova et al., "Microanatomical and biochemical origins of normal and precancerous cervical autofluorescence using laser-scanning fluorescence confocal microscopy," *Photochem. Photobiol.* **77**(5) 550–555 (2003).
4. P. P. Provenzano et al., "Collagen density promotes mammary tumor initiation and progression," *BMC Med.* **6**(11), 11 (2008).
5. S. K. Chang et al., "Analytical model to describe fluorescence spectra of normal and preneoplastic epithelial tissue: comparison with Monte Carlo simulations and clinical measurements," *J. Biomed. Opt.* **9**(3), 511–522 (2004).
6. D. C. Walker et al., "A study of the morphological parameters of cervical squamous epithelium," *Physiol. Meas.* **24**(1), 121–135 (2003).
7. M. H. Johnston, "Technology insight: ablative techniques for Barrett's esophagus: current and emerging trends," *Nat. Clin. Pract. Gastroenterol. Hepatol.* **2**(7), 323–330 (2005).
8. P. V. Butte et al., "Intraoperative delineation of primary brain tumors using time-resolved fluorescence spectroscopy," *J. Biomed. Opt.* **15**(2), 027008 (2010).
9. L. Marcu et al., "Detection of rupture-prone atherosclerotic plaques by time-resolved laser induced fluorescence spectroscopy," *Atherosclerosis* **204**(1), 156–164 (2009).
10. J. R. Lakowicz et al., "Intrinsic fluorescence from DNA can be enhanced by metallic particles," *Biochem. Biophys. Res. Commun.* **286**(5), 875–879 (2001).
11. J. Wu, M. S. Feld, and R. P. Rava, "Analytical model for extracting intrinsic fluorescence in turbid media," *Appl. Opt.* **32**(19), 3585–3595 (1993).
12. M. G. Müller et al., "Intrinsic fluorescence spectroscopy in turbid media: disentangling effects of scattering and absorption," *Appl. Opt.* **40**(25), 4633–4646 (2001).
13. G. M. Palmer and N. Ramanujam, "Monte-Carlo-based model for the extraction of intrinsic fluorescence from turbid media," *J. Biomed. Opt.* **13**(2), 024017 (2008).
14. S. C. Kanick et al., "Extraction of intrinsic fluorescence from single fiber fluorescence measurements on a turbid medium," *Opt. Lett.* **37**(5), 948–950 (2012).
15. G. M. Palmer and N. Ramanujam, "Monte Carlo-based inverse model for calculating tissue optical properties. Part I: theory and validation on synthetic phantoms," *Appl. Opt.* **45**(5), 1062–1071 (2006).
16. M. Müller and B. H. Hendriks, "Recovering intrinsic fluorescence by Monte Carlo modeling," *J. Biomed. Opt.* **18**(2) 027009 (2013).
17. Q. Wang et al., "Condensed Monte Carlo modeling of reflectance from biological tissue with a single illumination-detection fiber," *IEEE Sel. Top. Quantum Electron.* **16**(3) 627–634 (2010).
18. V. N. Du Le et al., "Vascular contrast in narrow band and white light imaging," *Appl. Opt.* **53**(18), 4061–4071 (2014).
19. Q. Fang and D. A. Boas, "Monte Carlo simulation of photon migration in 3D turbid media accelerated by graphics processing units," *Opt. Express* **17**(22), 20178–20190 (2009).
20. J. Chen, Q. Fang, and X. Intes, "Mesh-based Monte Carlo method in time-domain widefield fluorescence molecular tomography," *J. Biomed. Opt.* **17**(10) 106009 (2012).
21. Q. Fang, "Mesh-based Monte Carlo method using fast ray-tracing in Plücker coordinates," *Biomed. Opt. Express* **1**(1), 165–175 (2010).
22. K. R. Diamond, T. J. Farrell, and M. S. Patterson, "Measurement of fluorophore concentrations and fluorescence quantum yield in tissue-simulating phantoms using three diffusion models of steady-state spatially resolved fluorescence," *Phys. Med. Biol.* **48**(24), 4135–49 (2003).
23. D. J. Cuccia et al., "Quantitation and mapping of tissue optical properties using modulated imaging," *J. Biomed. Opt.* **14**, 024012 (2009).
24. J. C. Finlay and T. H. Foster, "Recovery of hemoglobin oxygen saturation and intrinsic fluorescence with a forward-adjoint model," *App. Opt.* **44**(10), 1917–1933 (2005).
25. A. Kim et al., "Quantification of in vivo fluorescence decoupled from the effects of tissue optical properties using fiber-optic spectroscopy measurements," *J. Biomed. Opt.* **15**(6), 067006 (2010).
26. C. L. Hoy et al., "Method for rapid multidiameter single-fiber reflectance and fluorescence spectroscopy through a fiber bundle," *J. Biomed. Opt.* **18**(10), 107005 (2013).
27. V. N. Du Le et al., "Measurements of extrinsic fluorescence in intralipid and polystyrene microspheres," *Biomed. Opt. Express* **5**(8), 2726–2735 (2014)
28. T. A. Middelburg et al., "Correction for tissue optical properties enables quantitative skin fluorescence measurements using multi-diameter single fiber reflectance spectroscopy," *J. Dermatol. Sci.* **79**(1), 64–73 (2015).

29. R. B. Saager et al., "Quantitative fluorescence imaging of protoporphyrin IX through determination of tissue optical properties in the spatial frequency domain," *J. Biomed. Opt.* **16**(12), 126013 (2011).
30. U. Sunar et al., "Quantification of PpIX concentration in basal cell carcinoma and squamous cell carcinoma models using spatial frequency domain imaging," *Biomed. Opt. Express* **4**(4), 531–537 (2013).
31. Q. Zhang et al., "Turbidity-free fluorescence spectroscopy of biological tissue," *Opt. Lett.* **25**(19), 1451–1452 (2000).
32. B. W. Pogue and M. S. Patterson, "Review of tissue simulating phantoms for optical spectroscopy, imaging and dosimetry," *J. Biomed. Opt.* **11**(4), 041102 (2006).
33. N. Rajaram et al., "Design and validation of a clinical instrument for spectral diagnosis of cutaneous malignancy," *Appl. Opt.* **49**(2), 142–152 (2010).
34. Q. Wang et al., "Broadband ultraviolet-visible optical property measurement in layered turbid media," *Biomed. Opt. Express* **3**(5), 1226–1240 (2012).
35. N. Rajaram, T. H. Nguyen, and J. W. Tunnell, "Lookup table–based inverse model for determining optical properties of turbid media," *J. Biomed. Opt.* **13**(5), 050501 (2008).
36. T. R. Wagner, W. G. Houf, and F. P. Incropera, "Radiative property measurements for India ink suspensions of varying concentration," *Solar Energy* **25**, 549–554 (1980).
37. H. Xu and M. Patterson, "Determination of the optical properties of tissue-simulating phantoms from interstitial frequency domain measurements of relative fluence and phase difference," *Opt. Express* **14**(14), 6485–6501 (2006).
38. Q. Liu, C. Zhu, and N. Ramanujam, "Experimental validation of Monte Carlo modeling of fluorescence in tissues in the UV-visible spectrum," *J. Biomed. Opt.* **8**(2), 223–236 (2003).
39. S. A. Ermilov et al., "Laser optoacoustic imaging system for detection of breast cancer," *J. Biomed. Opt.* **14**(2), 024007 (2009).
40. I. Barman et al., "Rapid and accurate determination of tissue optical properties using least-squares support vector machines," *Biomed. Opt. Express* **2**(3), 592–599 (2011).
41. B. Yu et al., "Diffuse reflectance spectroscopy of epithelial tissue with a smart fiber-optic probe," *Biomed. Opt. Express* **5**(3), 675–689 (2014).
42. D. Cappon et al., "Fiber-optic probe design and optical property recovery algorithm for optical biopsy of brain tissue," *J. Biomed. Opt.* **18**(10), 107004 (2013).
43. Z. Nie et al., "Hyperspectral fluorescence lifetime imaging for optical biopsy," *J. Biomed. Opt.* **18**(9), 096001 (2013).
44. Y. Yuan et al., "High throughput AOTF-based time-resolved fluorescence spectrometer for optical biopsy," *Opt. Lett.* **34**(7), 1132–1134 (2009).
45. P. G. Seybold, M. Gouterman, and J. Callis, "Calorimetric, photometric and lifetime determinations of fluorescence yields of fluorescein dyes," *Photochem. Photobiol.* **9**(3), 229–242 (1969).
46. D. Magde, R. Wong, and P. G. Seybold, "Fluorescence quantum yields and their relation to lifetimes of rhodamine 6G and fluorescein in nine solvents: improved absolute standards for quantum yields," *Photochem. Photobiol.* **75**(4), 327–334 (2002).
47. S. L. Jacques, R. Samatham, and N. Choudhury, "Rapid spectral analysis for spectral imaging," *Biomed. Opt. Express* **1**(1) 157–164 (2010).
48. M. S. Twardowski et al., "Modeling the spectral shape of absorption by chromophoric dissolved organic matter," *Mar. Chem.* **89**(1), 69–88 (2004).
49. X. Zhong, X. Wen, and D. Zhu, "Lookup-table–based inverse model for human skin reflectance spectroscopy: two-layered Monte Carlo simulations and experiments," *Opt. Express* **22**(2), 1852–1864 (2014).
50. J. M. Dixon, M. Taniguchi, and J. S. Lindsey, "PhotochemCAD. A computer-aided design and research tool in photochemistry and photobiology," *Photochem. Photobiol.* **81**(1), 212–213 (2005).
51. R. Nachabé et al., "Estimation of biological chromophores using diffuse optical spectroscopy: benefit of extending the UV-VIS wavelength range to include 1000 to 1600 nm," *Biomed. Opt. Express* **1**(5), 1432–1442 (2010).
52. S. L. Jacques, "Optical properties of biological tissues: a review," *Phys. Med. Biol.* **58**(11), R37 (2013).

Vinh Nguyen Du Le is a PhD student in the medical physics program at McMaster University (Hamilton, ON). He received a BSc degree (2009) and a MSc degree (2010) in biomedical engineering from the Catholic University of America (Washington, DC). He was a research fellow at the U. S. Food and Drug Administration from 2010 to 2012.

Michael S. Patterson is the director of medical physics at Juravinski Cancer Centre (Hamilton, ON). He received a BSc degree (1973) from Queen's University, a MSc degree (1976) from McMaster University, and a PhD degree (1984) from the University of Toronto.

Thomas J. Farrell is a medical physicist at the Juravinski Cancer Centre and the chair of the medical physics department at McMaster University. He received his PhD degree (1990) from McMaster University.

Joseph E. Hayward is a medical physicist at the Juravinski Cancer Centre and an associate professor of the medical physics department at McMaster University. He received his PhD degree (1993) in lasers and electro-optics in engineering physics from McMaster University.

Qiyin Fang is an associate professor of Engineering Physics and the chair of biophotonics at McMaster University. He received his BSc degree (1995) in physics from Nankai University, his MSc degree (1998) in applied physics, and his PhD degree (2002) in biomedical physics from East Carolina University.